Photo-Induced Shrinking of Aqueous Glycine Aerosol Droplets

Shinnosuke Ishizuka,[a,b,c ‡, *] Oliver Reich,[a, ‡] Grégory David,[a] and Ruth Signorell[a]*

[a] Laboratory of Physical Chemistry, ETH Zurich, Vladimir-Prelog-Weg 2, CH-8093, Zurich, Switzerland

[b] Institute of Advanced Research, Nagoya University, Nagoya 046-8601, Japan

[c] Institute of Space-Earth Environmental Research, Nagoya University, Nagoya 046-8601, Japan

ABSTRACT: Due to their small size, micrometer and submicron sized solution droplets can respond differently to physical and chemical processes compared with extended bulk material. Using optically trapped micrometer sized aqueous glycine droplets, we demonstrate a photo-induced degradation of glycine upon irradiation with visible light, even though molecular glycine does not absorb light in the near UV/vis range to any significant extent. This reaction is observed as photo-induced shrinking of the droplet, which we characterize by analyzing the elastic light scattering and the Raman spectrum of the droplet over the course of the reaction. We find the volume to shrink with a constant rate over the major part of the shrinking process. This indicates the presence of a rate limiting photo-catalyst, which we attribute to mesoscopic glycine clusters in the droplet solution. Our findings relate to previous reports about enhanced absorption and fluorescence rates of amino acid solutions. However, to the best of our knowledge, this is the first experimental evidence of a photochemical pathway facilitated by mesoscopic clusters. Light interaction with such mesoscopic photoactive molecular aggregates might be more important for aerosol photochemistry than previously anticipated.

* rsignorell@ethz.ch, ishizuka.shinnosuke.a3@f.mail.nagoya-u.ac.jp

‡ S.I. and O.R. contributed equally to this work.

1. INTRODUCTION

Aerosols, dispersions of solid and liquid particles in a gas, are ubiquitous in Earth's atmosphere and as such play an important role for many atmospheric processes (Boucher et al., 2013; PöSchl and Shiraiwa, 2015). Size, chemical composition, viscosity and thermodynamic phase of aerosol particles respond to their environment including the surrounding gas species, temperature, humidity (Bones et al., 2012; Zieger et al., 2017; Tang et al., 1997; Swietlicki et al., 2008) and light irradiation (PöSchl and Shiraiwa, 2015; Cremer et al., 2016; Walser et al., 2007; Corral Arroyo et al., 2022). Particular attention has been paid to their chemistry distinct from that in the bulk, a phenomenon possibly arising from high surface to volume ratio of aerosol particles and the accessibility to highly supersaturated states (Altaf et al., 2016; Kucinski et al., 2019; Bzdek and Reid, 2017). Various chemical reactions have been shown to be accelerated in microdroplets (Cremer et al., 2016; Lee et al., 2015; Girod et al., 2011), with some reactions being exclusive to the droplet phase (Lee et al., 2019). These unique reactors can act as medium for the birth, growth and degradation of atmospherically relevant particles (Ruiz-Lopez et al., 2020), and be utilized for organic synthesis (Bain et al., 2017). Chemical processes in prebiotic aerosols have also been proposed as potential mechanisms for the origin of life (Tervahattu et al., 2004). However, molecular processes leading to the anomalous chemistry in micrometer and submicron aerosol particles are still largely unknown. Although some processes may be ascribed to the discontinuous and asymmetric intermolecular interactions at the particle surface (Ruiz-Lopez et al., 2020), the microphysical origins behind many of the aforementioned particle specific phenomena are still not adequately explored.

Glycine is an amino acid that acts as precursor to proteins and fulfills a number of other biological functions (Arnstein, 1954; Hall, 1998; Jackson, 1991). With its small size and simple structure, glycine often serves as a proxy for other amino acids and physiologically relevant molecules, and as such has been studied extensively in the past. It is generally accepted that molecular glycine does not absorb light in the near UV/vis range, similar to other amino acids (Bhat and Dharmaprakash, 2002). However, it has been shown that their optical properties change when glycine molecules arrange themselves into mesoscopic clusters by forming hydrogen bond networks (Terpugov et al., 2021). Furthermore, these formations respond to light irradiation in non-trivial ways which can be exploited to induce long range order inside the glycine solution (Alexander and Camp, 2019; Sugiyama et al., 2012; Zaccaro et al., 2001; Garetz et al., 2002; Urquidi et al., 2022) on a scale of up to millimeters (Yuyama et al., 2010). While these interactions have the potential to change the optical properties of glycine ensembles significantly and to enable new photochemical reaction pathways, there has been little experimental evidence for such reactions so far.

In this work, we study the response of aqueous glycine droplets to irradiation by visible light. We observe the shrinking of optically trapped micrometer sized glycine droplets, which can be unambiguously attributed to the exposure to the trapping laser with wavelength 532 nm. To the best of our knowledge, this interaction has not been reported before. We characterize it here with particular focus on the shrinking rate and its dependence on the

light intensity. To explain our results, we discuss possible reaction schemes based on the available experimental data. Although further data is needed to elucidate the exact photochemical pathways of the observed reaction, these findings demonstrate the existence of a photochemical reaction for molecules which previously have been considered photochemically inert at visible wavelengths.

2. METHODS

Dual beam optical traps are widely used to confine and isolate single particles (Ashkin, 1997; Gong et al., 2018; Čižmár et al., 2005; Esat et al., 2018; Reich et al., 2020). The counter-propagating tweezers (CPT) setup for trapping aqueous glycine droplets is shown in Fig. 1 and consists of a continuous green laser beam (Novanta Photonics Opus 532 6W), which is expanded and then split into two beams of equal power. These two beams are aligned counter-propagating on a single axis and focused into the trapping cell, where a single droplet is trapped between the two focii.

The droplets are generated from 1.0 M or 2.0 M aqueous solutions of glycine (purity 100%, HPLC certificate, Sigma-Aldrich G7126) using a commercial atomizer (TSI 3076) with pressurized, humidified nitrogen gas (purity 5.0). We performed additional elementary and HPLC analyses of the glycine and the glycine solutions. The results showed no indication of any trace impurities absorbing in the visible range. On this basis, we conclude that our samples do not contain any contaminants that could act as photosensitizer for photochemical reactions (see below). A system of copper tubings directs the spray of particles into the trapping cell, where the droplets agglomerate at the designated trapping position. The humidification of the nitrogen flow is necessary to ensure that the droplets reach the trapping position in the liquid state. The trapping cell is filled with nitrogen gas (purity 5.0) and a steady nitrogen flow formed by combining wet and dry nitrogen with adjustable flow ratios is used to control the relative humidity (RH) in the cell. For the experiments reported here, the RH is set at 77 ± 3 % well above the efflorescence RH of glycine at approximately 55 % (Chan et al., 2005). At this RH, the droplet solution is supersaturated with an estimated glycine concentration of 60 % in mass (Chan et al., 2005), corresponding to approximately 5 M. Temperature and RH inside the trapping cell are monitored by a sensor (Sensirion SHT35) placed a few millimeters away from the trapping position. When the agglomerated particle reaches a size of approximately 2-3μm in radius, the remainder of the droplets in the cell are flushed out with nitrogen for 20-30 minutes to ensure that only the trapped droplet remains in the cell. After flushing, the power of the trapping laser is kept constant until the end of the measurement.

The particle shrinking is monitored by imaging the polarization resolved two-dimensional angular optical scattering (polarization resolved TAOS) of the particle (Parmentier et al., 2022), as shown in Fig. 2. The TAOS image is obtained by collecting the elastically scattered light of the trapping beams under a scattering angle of $90 \pm 24°$ with an objective (Mitutoyo 20x NA 0.42). The parallel and perpendicular polarization components with respect to the scattering plane (TAOS PPol and TAOS SPol) are separated using a polarization beam splitter and recorded with separate CMOS cameras (Thorlabs DCC1545M). The scattering intensity for each polarization is calculated from the average of the respective TAOS image and recorded over time. At specific times, the shrinking spherical particle reaches a size at which it is in resonance with the light of the trapping beams, which corresponds to a Mie resonance (Bohren and Huffman, 2008). From the comparison of the recorded evolution of the polarization resolved scattering intensity to simulations using Mie theory, the size of the particle can be determined at the specific

79   times. Fig. 3 shows an example of such a TAOS analysis. The values of the size at the discrete points in time,

80   obtained from the times where the particles experience a Mie resonance, can then be interpolated with high accu-

81   racy to obtain the full size evolution of the particle over the course of the measurement.

82

83   The molecular composition of the particle is monitored by continuous recording of Raman spectra (David et al.,

84   2020) during the shrinking process. To this end, the light scattered by the particle is collected under a scattering

85   angle of $90 \pm 24°$ by a second objective and fiber coupled into a low noise, high sensitivity spectrograph (Andor

86   KY-328i-A). The inelastically scattered light is analyzed in the range 540-680 nm which corresponds to Raman

87   shifts of 280-4100 cm^{-1}. This range contains in particular the O-H symmetric stretching mode of water (ν_2-H_2O,

88   2700-3750 cm^{-1}) as well as several vibrational modes of glycine, which we exploit for the characterization of the

89   molecular composition (see later data for an example).

90
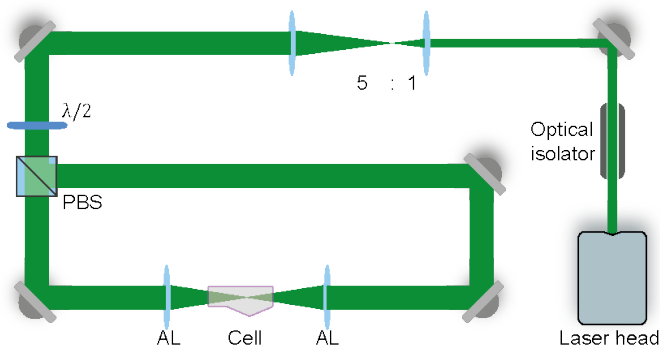
91

92   **Figure 1** Counter-propagating tweezers setup. The laser beam is first expanded by a factor of 5 and then split into

93   two beams by the polarizing beam splitter (PBS). The half-waveplate ($\lambda/2$) rotates the polarization to 45° with

94   respect to the axes of the PBS to ensure equal power splitting between the two beams. The beams are aligned on

95   a single axis and focused into the trapping cell using two aspherical lenses (AL). An optical isolator introduced

96   at the start of the beam path prevents unwanted optical feedback into the laser head.

97
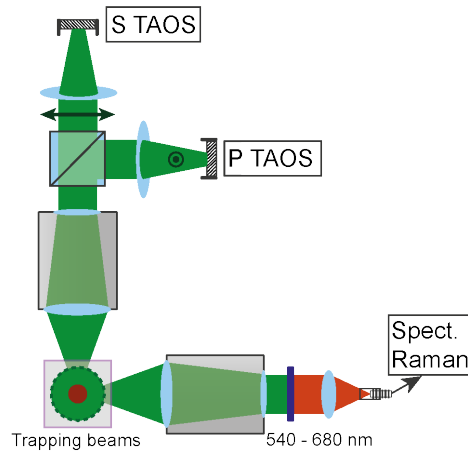
Figure 2 Setup for TAOS imaging and Raman spectroscopy. The trapping beams run perpendicular to the figure plane. The scattered light of the trapping beams is collected horizontally and vertically at a scattering angle of 90 ± 24°. The vertical beam is split into parallel and perpendicular polarized light with respect to the scattering plane and the respective beam is loosely focused on a CMOS camera (P TAOS and S TAOS respectively). The horizontal beam is filtered for the spectral range of 540 – 680 nm and fiber coupled into a low noise, high sensitivity spectrometer (Spect. Raman) for measurement of the Raman spectrum.
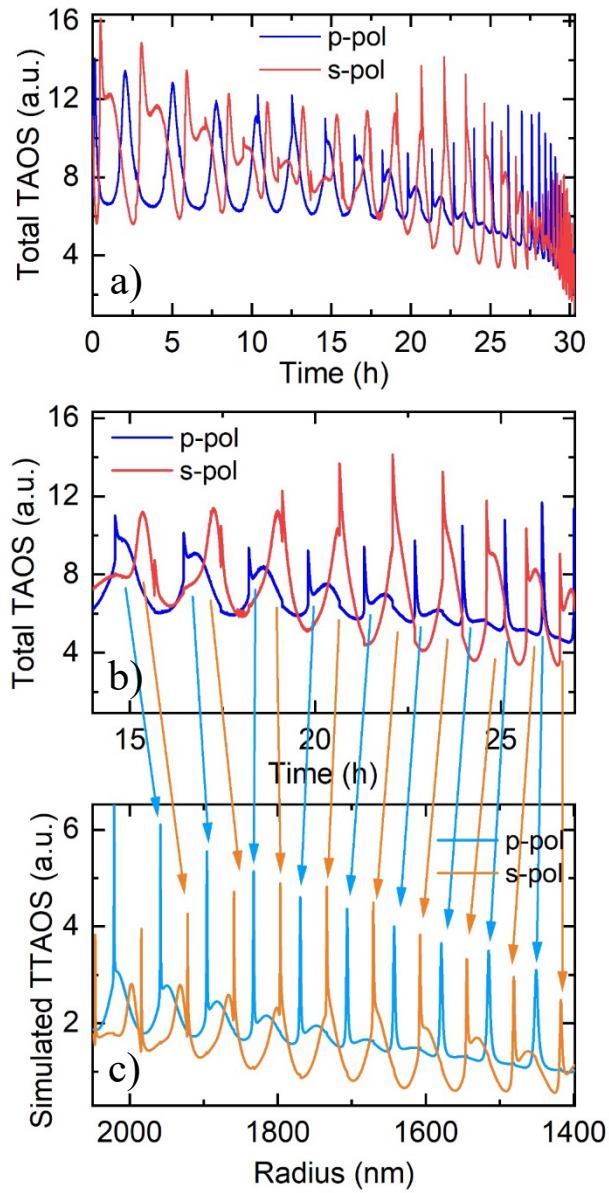
Figure 3 Analysis of the two-dimensional angular optical scattering spectrum (TAOS). **a)** Experimental polarization resolved total TAOS signal over time. **b)** Zoom on a specific time interval for clarity **c)** Simulated polarization resolved total TAOS signal as function of particle radius in the specific time interval. Arrows indicate the peak assignment based on the similarities between the peak shapes.

3. RESULTS AND DISCUSSION

The shrinking of the aqueous glycine droplets over time is shown in Fig. 4 for three representative examples. The droplets are trapped using different laser powers, which affects the rate at which their volume is decreasing. For all laser powers, the volume is observed to shrink linearly with time over a large portion of the shrinking process. After a certain point ('point of acceleration'), when the droplet has lost 60 – 80 % of its volume, the shrinking suddenly accelerates, only to continue again approximately linearly with time, albeit at a higher rate.
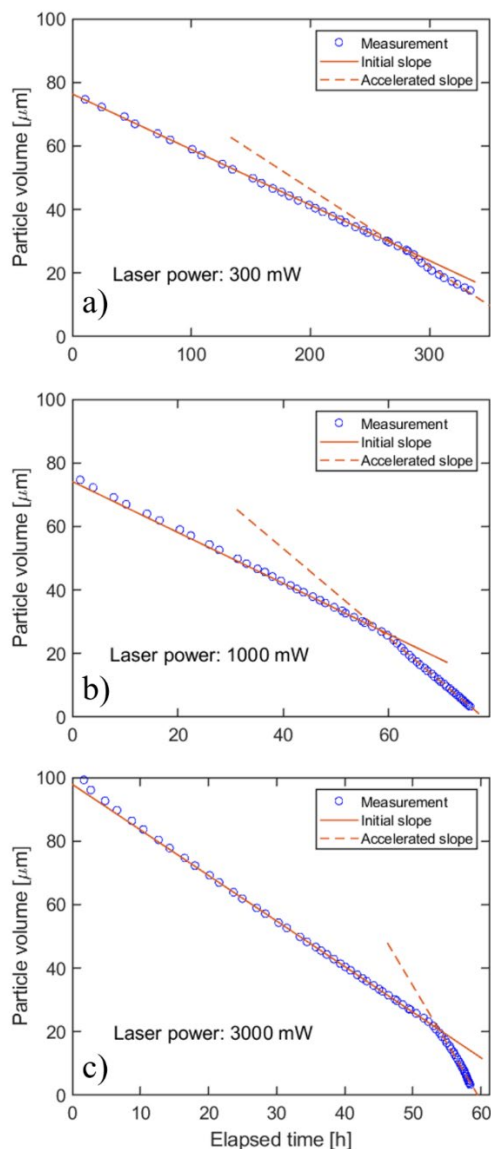
Figure 4 Volume shrinking of glycine droplets as a function of time. **a)** Droplet trapped at 300 mW nominal laser power **b)** droplet trapped at 1000 mW nominal laser power **c)** droplet trapped at 3000 mW nominal laser power. At higher power, the shrinking proceeds faster (visible by the lager slopes). Solid and dashed lines indicate the best linear fit before and after the acceleration of the shrinking observed at approximately **a)** 280 h, **b)** 59 h and **c)** 53 h.

124   To quantify the dependence of the shrinking rate on the light intensity incident on the particle, a linear fit is
125   performed on the data before and after the point of acceleration. Since between different experiments, the align-
126   ment of the optical trap, and hence the focusing of the laser light on the particle, is subject to temporal mechanical
127   drifts, the nominal laser power used for trapping of the droplets is not an optimal indicator for the incident inten-
128   sity. Instead, we use the intensity of the scattered light as a measure that is proportional to the incident light
129   intensity. The intensity of the scattered light is obtained from the average signal of the TAOS PPol and SPol
130   images during the time of the droplet shrinking. To ensure consistency between the different experiments, the
131   average of the light intensity is taken over the same volume interval of [65.4, 51.0] μm^3 (radius [2.5, 2.1] μm) for
132   all droplets. This interval corresponds to the interval for which we obtained data for most droplets. Fig. 5 shows
133   the resulting initial shrinking rates as function of light intensity. The shrinking rate is observed to be proportional
134   to the light intensity, confirming that the shrinking is induced by the trapping laser at a wavelength of 532 nm.
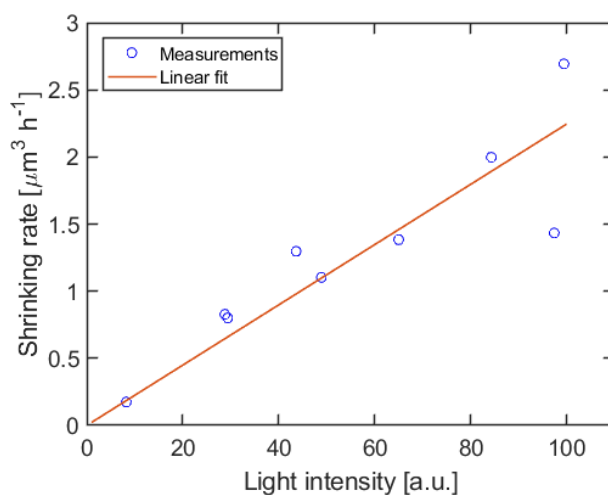

135

136   **Figure 5** Fitted shrinking rate as function of light intensity. The solid line indicates the best linear fit through
137   the origin.

138   To gain further insight into the shrinking mechanism, we analyze the evolution of the Raman spectra over the
139   course of the shrinking process. A representative example of such an evolution is shown in Fig. 6. For Raman
140   spectra of single spherical particles, so called morphology dependent resonances, or whispering gallery modes
141   (WGMs) (Oraevsky, 2002), are superimposed on the molecular signals. To separate the WGMs from the molecular
142   signal of interest, the Raman spectra are normalized and stacked in chronological order from left to right, as shown
143   in Fig. 6a. The WGMs show up as a manifold of thin slanted lines bending towards lower wavenumbers with
144   increasing time as the droplet shrinks. Molecular band positions on the other hand are independent of particle
145   size, and are identified as horizontal lines in the evolution of the Raman spectra.

146

147   From Fig. 6a it is evident that the molecular Raman signal remains qualitatively the same, indicating that no
148   significant change in the molecular composition takes place in the droplet over the course of the shrinking process.
149   This behavior is observed for all investigated droplets. Since the particle loses the major part of its volume during

150 the shrinking, this implies that glycine is removed from the droplet as a consequence of chemical reaction (*vide*
151 *infra*). As the water vapor pressure of the droplet is given by the surrounding RH of 77 % and therefore has to
152 remain constant, the removal of glycine from the droplet must be accompanied by the evaporation of water in
153 order to maintain the equilibrium glycine concentration. A quantitative analysis of the Raman spectrum (Fig. 6b)
154 reveals that the spectral intensity of glycine modes with respect to the O-H stretching mode of water remains
155 constant, confirming a constant concentration of glycine molecules during the shrinking process. The measure-
156 ment ends when the particle becomes too small for stable trapping, and therefore leaves the optical trap.

157

158
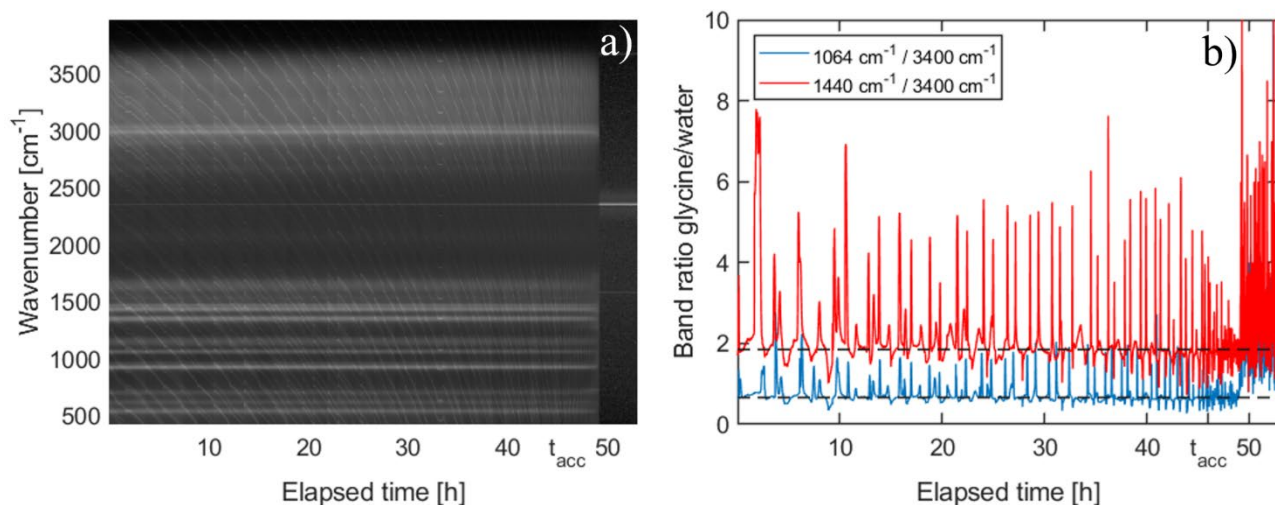
Figure 6 Temporal evolution of Raman signal during droplet shrinking. **a)** Normalized Raman spectra stacked
chronologically from left to right. The molecular Raman bands are visible as horizontal straight white lines on the
dark background. The finer, slanted and curved lines correspond to whispering gallery modes. After approxi-
mately 49 h, the particle leaves the optical trap as it reaches a size that is too small for trapping, and only back-
ground is recorded. The band remaining afterwards at 2323 cm^{-1} corresponds to the nitrogen gas in the trapping
cell. **b)** Ratio of the molecular glycine bands centered at 1064 cm^{-1} and 1440 cm^{-1} to the water band at around
3400 cm^{-1}. Peaks and dips in the graphs correspond to spectra where a whispering gallery mode is superimposed
on the glycine signal and the water signal, respectively, and are not relevant for the molecular composition. The
dashed horizontal lines are a guide to the eye. In this example, the acceleration of the droplet shrinking is observed
at $t_{acc} = 46$ h. From this point in time onwards until the particle is lost, the faster shrinking leads to more frequent
WGMs perceived as an apparent increase of noise in the data.

170 Aqueous droplets which contain a stable non-volatile solute do not shrink over time when they are optically
171 trapped (see Supplementary Section S1 for an example). The observation of droplet shrinking in the case of dis-
172 solved glycine proves that glycine does not remain stable inside the droplet solution. Furthermore, the linear
173 dependence of the shrinking rate on the light intensity (Fig. 5) proves that the observed shrinking is induced by
174 the laser light. In particular, the volume shrinking rate increases from 0.18 to 2.25 µm^3 h^{-1} when the light intensity

is increased by the same relative amount, thus spanning over one order of magnitude. This observation is intriguing as aqueous glycine is not known to absorb light in the visible range, similar to other amino acids (Bhat and Dharmaprakash, 2002). In addition, the linear dependence between shrinking rate and light intensity rules out the possibility of multiphoton absorption, which might otherwise populate energetically excited states of glycine to induce chemical reactions. The fact that the observed shrinking is driven by the incident light indicates a photochemical reaction or photothermal processes occurring in the aqueous glycine droplet. As is shown in the following however, photothermal processes can be ruled out by our experimental data.

The observation of a constant shrinking rate over a large portion of the experiments (Fig. 4) provides another important piece of information, as this allows us to rule out some of the possible shrinking mechanisms. For instance, assuming some residual absorption of light at 532 nm by the droplet solution, one might argue that the shrinking is a consequence of enhanced evaporation due to the droplet heating by the laser. The evaporation of glycine from the droplet can be approximated by the Hertz-Knudsen equation:

$$\frac{\mathrm{d}N}{\mathrm{d}t} = S \cdot \frac{\alpha p}{\sqrt{2\pi MRT}} \tag{1}$$

where $\frac{\mathrm{d}N}{\mathrm{d}t}$ is the molar evaporation rate of glycine, S is the droplet's surface, p is the partial pressure and M is the molar mass of glycine, R the gas constant, T the temperature and α a heuristic sticking coefficient with values between 0 and 1. It is evident from Eq. (1) that the rate of shrinking by evaporation should scale with the surface area of the droplet, and that in this case a deceleration of the shrinking should be observed over time, contrary to the experimental data. Moreover, any heating by laser light absorption would at most lead to a very small temperature rise due to the efficient cooling by the surrounding gas (see Supplementary Section S2 for an upper estimate of the temperature increase). In addition to these arguments, if evaporation were significant, some evaporation should still be observable even at low light intensity, where the heating of the droplet is negligible and hence any deviations form room temperature can be neglected. As seen from Fig. 5 however, there is no shrinking observable for low light intensities. We can therefore rule out evaporation as the dominant shrinking mechanism.

The observation of a constant shrinking rate also excludes photochemical reactions in which molecular glycine directly absorbs photons:

$$\mathrm{Gly(aq)} + h\nu \rightarrow \mathrm{P(aq)} \rightarrow \mathrm{P(g)}, \tag{2}$$
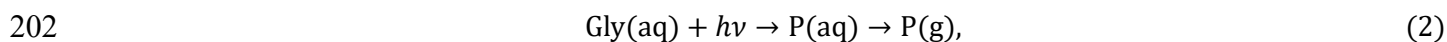
where Gly(aq) is a solvated glycine molecule, $h\nu$ is the energy of the incoming photon and P is the reaction product that is removed from the droplet (aq) into the surrounding gas phase (g) afterwards. As mentioned above. molecular glycine is considered non-absorbing at 532 nm. However, if we nevertheless assume that molecular glycine could be very weakly absorbing as in Eq. (2), the photon density inside the droplet would be constant over the course of the photochemical reaction. Earlier studies (Parmentier et al., 2021; Corral Arroyo et al., 2022) show that no significant size dependence of the optical confinement is observed for weakly absorbing particles in the micrometer- and submicrometer-size ranges. Hence, the first step in Eq. (2) would be pseudo-first order, for which

210   the reaction rate is proportional to the concentration of glycine molecules in the droplet. Therefore, one would
211   expect a decrease in the observed shrinking rate over time, which contradicts the experimental observation.

212

213   The examples above illustrate that any mechanism, in which glycine molecules directly absorb incoming photons,
214   cannot explain the constant shrinking rates. This implies that a more intricate reaction must take place in the
215   droplet. We suggest the following simplified scheme with an additional reaction partner M:

$$M + h\nu \rightarrow M^* \tag{3}$$

$$M^* + Gly \rightarrow M + P \tag{4}$$
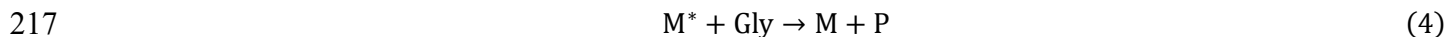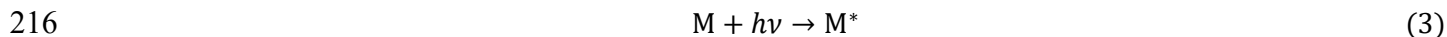
218   where M^* denotes a photoexcited state of M, and P is the reaction product of glycine in the presence of this pho-
219   toexited species. This scheme represents a mediated reaction in which the reaction partner M is activated by light
220   absorption, and then reacts with glycine and returns back to the ground state. M shows the characteristics of a
221   photosensitizer (Corral Arroyo et al., 2018; George et al., 2015; Wang et al., 2020; Rapf and Vaida, 2016), which
222   is not consumed during the reaction, and therefore the amount of M remains constant in the droplet. We further
223   assume that the light absorption of the photosensitizer M is the rate limiting step, i.e., that Eq. (3) proceeds much
224   slower than Eq. (4). This is equivalent to requiring that M is only weakly absorbing, or that the concentration of
225   M in the droplet is low. Since the amount of M in the rate limiting step (Eq. (3)) remains constant during the
226   shrinking process, so does M^* (quasistationary), resulting in a constant rate of degradation of Gly (Eq. (4)). As-
227   suming that the absolute concentration of M is much smaller than that of Gly at all times, and therefore has no
228   relevant effect on the equilibrium water vapor pressure of the droplet, the volume shrinking rate is predicted to be
229   constant in accordance with the experimental data.

230

231   Although the proposed mechanism in Eq. (3) and (4) concurs with the observed constant shrinking rates, it does
232   not yet specify the nature of the photosensitizer and its reaction with glycine. We first discuss potential candidates
233   for the photosensitizer. Contamination during the preparation of the different aqueous glycine solutions used in
234   this study was minimized by using pure substances (glycine purity $\geq$ 99 %, water resistivity 18.2 MΩ·s). No
235   correlation between the shrinking rates in Fig. 5 and the age of the solution at the time of the measurements was
236   observed, which indicates that there is no accumulation of photoactive contaminants in the solution after the
237   preparation. We therefore argue that contamination is not the origin of the photosensitizer.

238

239   It is evident from the previous discussion that the photosensitizer must possess an absorption band at 532 nm,
240   which is not the case for single solvated glycine molecules. The optical properties of molecules may change
241   however when forming intermolecular bonds, e.g. leading to an enhancement of the absorption and fluorescence
242   in the case of protein aggregates (Homchaudhuri and Swaminathan, 2004; Shukla et al., 2004; Chan et al., 2013;
243   Pinotsi et al., 2013) and amino acid clusters (Chen et al., 2018). For glycine solutions in particular, observations
244   of light absorption in the near UV/vis range have been attributed to the presence of mesoscopic clusters (Jawor-

Baczynska et al., 2013; Zimbitas et al., 2019), specifically due to the formation of hydrogen bonds between individual molecules (Terpugov et al., 2021).

Mesoscopic clusters occur naturally in both undersaturated and supersaturated glycine solutions, though a kinetic barrier may have to be overcome for their formation (Jawor-Baczynska et al., 2013).). A similar barrier needs to be overcome to dissolve these clusters. Hence the clusters can remain kinetically stable even if the number of glycine monomers decreases. The average size of the mesoscopic clusters, typically of the order of 100 nm for bulk solutions, depends not only on the monomer concentration but also on the history of the sample, indicating that the clusters do not necessarily remain in thermodynamic equilibrium after formation (Jawor-Baczynska et al., 2013). Based on these observations, we propose that the photo-induced droplet shrinking is mediated by light absorption of mesoclusters in the glycine solution. These mesoclusters remain kinetically stable during the droplet shrinking, despite the decrease of the absolute number of glycine monomers (i. e. constant glycine monomer concentration). Hence, these clusters act as stable photosensitizers inside the droplets, in accordance with the observed constant shrinking rate. The observation of a constant initial shrinking rate thus allows us to narrow down the possible reaction mechanisms at work in the droplets. Alternative schemes might be conceivable, such as the existence of several reaction partners for glycine. However, there is no further experimental evidence in favor of more complex alternatives to the simple mechanism proposed (Eq. (3) and (4)). Furthermore, as pointed out above, mesoscopic glycine clusters match the requisite characteristics of the proposed photosensitizer, and are therefore likely candidates. To pursue the argument, let us further discuss the role of the mesoscopic clusters in the observed acceleration of the droplet shrinking.

The acceleration of the droplet shrinking proceeds relatively promptly at the point of acceleration when the particle has lost a typical amount of 75 % of its volume (Fig. 4). Assuming that the total number of mesoclusters remains approximately constant (M in Eqs.(3) and (4)), their concentration has increased by an approximate factor of 4 at this point. The sudden nature of the shrinking acceleration hints at a phase transition inside the particle. In particular, the increase in nanocluster concentration may trigger the separation of a dense cluster phase inside the droplets as part of a liquid-liquid phase transition. While a definite conclusion has to await more detailed microscopic investigations, we present the following arguments in favor of this explanation. Mesoscopic clusters in aqueous solutions are known to interact with focused light irradiation by assembling in the focal point of the light beam due to the optical force that acts on the individual clusters (Sugiyama et al., 2012). This mechanism is the basis of laser-induced phase transitions(Alexander and Camp, 2019), in the particular case of glycine both for liquid-liquid phase separation (Sugiyama et al., 2012; Yuyama et al., 2010) and solid crystal nucleation (Sugiyama et al., 2012; Alexander and Camp, 2019; Yuyama et al., 2010; Zaccaro et al., 2001; Garetz et al., 2002). It should be noted at this point that the spot size in the focus of our optical trap is slightly larger (5 μm) than the typical droplet size, and that therefore, it might appear unlikely that the electromagnetic field gradient is strong enough to induce cluster aggregation in our case. However, micrometer sized droplets exhibit a large variance in the spatial distribution of the internal light field, owing to the nanofocusing effect (Cremer et al., 2016; Corral Arroyo

282 et al., 2022), which can provide the field gradients necessary for aggregation. If in the case of our trapped droplets,

283 the acceleration is due to a phase transition, it would likely be assisted by the light irradiance. One would therefore

284 expect a dependence of the observed shrinking acceleration on the incident light intensity. Fig. 7 shows the meas-

285 ured acceleration ratio, that is, the ratio between the shrinking rate after to before the point of acceleration, as a

286 function of light intensity. From this data it is evident that the ratio increases with higher light intensity, which

287 agrees with our explanation of a light-induced phase transition. Since in this scheme, the clusters are expected to

288 aggregate in the regions of high light intensity after reaching a critical concentration, this would lead to a larger

289 absorption rate and thus a larger subsequent reaction rate, in agreement with the observation. Further studies will

290 be necessary to provide conclusive evidence for this explanation.

291
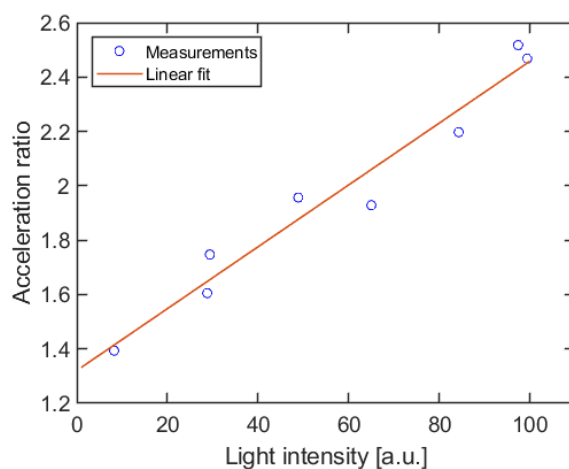
292

293 **Figure 7** Acceleration of droplet shrinking versus light intensity. The solid line represents the best linear fit

294 through the measurement data.

295 More data will also be required to understand the specifics of the interaction between the photosensitizer and the

296 solvated glycine molecules in Eq. (4). Here, we can only provide a qualitative discussion based on the available

297 data. The Raman spectra (Fig. 6) show no detectable change in the molecular composition, even after the droplet

298 has lost the major part of its volume during the shrinking process. Since this observation rules out the accumula-

299 tion of reaction products in the droplets over time, the reaction products must be small, volatile compounds that

300 quickly evaporate into the surrounding gas phase. Known degradation mechanisms of glycine and other amino

301 acids in aqueous solution proceed via reaction with radical species, in particular solvated electrons e_{solv}^- and hy-

302 droxyl $^\bullet$OH radicals (Moenig et al., 1985; Garrison, 1964, 1972), which form as part of a photosensitized reaction

303 with chromophoric organic matter in water (Lundeen et al., 2014; Sun et al., 2018; Mopper and Zika, 1987).

304 Currently, our data does not allow us to distinguish between different degradation pathways.

305

306 4. CONCLUSIONS

307 We have demonstrated that single micrometer sized aqueous glycine droplets respond to the illumination with

308 laser light of 532 nm by shrinking, despite the fact that molecular glycine does not absorb in the near UV/vis

14

range. Most remarkably, the volume shrinking rate remained constant over the major part of the shrinking process. This indicates a photo-induced decay of glycine molecules in the presence of a rate limiting catalyst, or photosensitizer, and the subsequent evaporation of small, volatile reaction products. Based on the available literature data, we propose that intrinsic mesoscopic clusters of glycine molecules formed by hydrogen bonding in the aqueous solution are the most plausible candidates for this photosensitizer. The presence of mesoscopic glycine clusters would also explain the sudden acceleration of the shrinking rate occurring at a volume loss of ~75 %. Because of its dependence on the light intensity, we attribute this sudden rate change to arise from the interaction of the mesoclusters with the incident light, possibly initiating a light-induced phase transition.

This study provides yet another example of the non-trivial interactions of light with aqueous glycine solutions (Alexander and Camp, 2019; Sugiyama et al., 2012; Zaccaro et al., 2001; Garetz et al., 2002; Yuyama et al., 2010), which facilitate previously undiscovered reaction pathways - interactions that are likely not exclusive to glycine. Light harvesting by and light interaction with such mesoscopic photosensitizers in aerosol droplets might also have played a role in the formation of more complex organic molecules under prebiotic conditions. Further investigations are needed to shed light on the specifics of the observed phenomena, and to yield new insight into the underlying reaction mechanisms, which remain elusive in part. Studying solutions in micrometer sized droplets (attoliter volumes) using high laser powers offers the advantage of much higher sensitivity to photo-induced reactions than typically achievable with bulk solutions.

Data Repository

The data that support our findings are deposited on the ETH Research Collection under https://doi.org/xx.

References

340 Alexander, A. J. and Camp, P. J.: Non-photochemical laser-induced nucleation, The Journal of chemical physics, 150, 040901, 2019.

341 Altaf, M. B., Zuend, A., and Freedman, M. A.: Role of nucleation mechanism on the size dependent morphology of organic aerosol, Chem.
342 Commun., 52, 9220-9223, 2016.

343 Arnstein, H.: The metabolism of glycine, in: Adv. Protein Chem., Elsevier, 1-91, 1954.

344 Ashkin, A.: Optical trapping and manipulation of neutral particles using lasers, Proceedings of the National Academy of Sciences, 94, 4853-
345 4860, 1997.

346 Bain, R. M., Sathyamoorthi, S., and Zare, R. N.: ″On‐droplet″ chemistry: the cycloaddition of diethyl azodicarboxylate and quadricyclane,
347 Angew. Chem., 129, 15279-15283, 2017.

348 Bhat, M. N. and Dharmaprakash, S.: Growth of nonlinear optical γ-glycine crystals, J. Cryst. Growth, 236, 376-380, 2002.

349 Bohren, C. F. and Huffman, D. R.: Absorption and scattering of light by small particles, John Wiley & Sons2008.

350 Bones, D. L., Reid, J. P., Lienhard, D. M., and Krieger, U. K.: Comparing the mechanism of water condensation and evaporation in glassy
351 aerosol, Proceedings of the National Academy of Sciences, 109, 11613-11618, 2012.

352 Boucher, O., Randall, D., Artaxo, P., Bretherton, C., Feingold, G., Forster, P., Kerminen, V.-M., Kondo, Y., Liao, H., and Lohmann, U.:
353 Clouds and aerosols, in: Climate change 2013: the physical science basis. Contribution of Working Group I to the Fifth Assessment Report
354 of the Intergovernmental Panel on Climate Change, Cambridge University Press, 571-657, 2013.

355 Bzdek, B. R. and Reid, J. P.: Perspective: Aerosol microphysics: From molecules to the chemical physics of aerosols, The Journal of
356 Chemical Physics, 147, 220901, 2017.

357 Chan, F. T., Schierle, G. S. K., Kumita, J. R., Bertoncini, C. W., Dobson, C. M., and Kaminski, C. F.: Protein amyloids develop an intrinsic
358 fluorescence signature during aggregation, Analyst, 138, 2156-2162, 2013.

359 Chan, M. N., Choi, M. Y., Ng, N. L., and Chan, C. K.: Hygroscopicity of water-soluble organic compounds in atmospheric aerosols: Amino
360 acids and biomass burning derived organic species, Environ. Sci. Technol., 39, 1555-1562, 2005.

361 Chen, X., Luo, W., Ma, H., Peng, Q., Yuan, W. Z., and Zhang, Y.: Prevalent intrinsic emission from nonaromatic amino acids and poly
362 (amino acids), Science China Chemistry, 61, 351-359, 2018.

363 Čižmár, T., Garcés-Chávez, V., Dholakia, K., and Zemánek, P.: Optical conveyor belt for delivery of submicron objects, Appl. Phys. Lett.,
364 86, 174101, 2005.

365 Corral Arroyo, P., David, G., Alpert, P. A., Parmentier, E. A., Ammann, M., and Signorell, R.: Amplification of light within aerosol particles
366 accelerates in-particle photochemistry, Science, 376, 293-296, 2022.

367 Corral Arroyo, P., Bartels-Rausch, T., Alpert, P. A., Dumas, S. p., Perrier, S. b., George, C., and Ammann, M.: Particle-phase photosensitized
368 radical production and aerosol aging, Environ. Sci. Technol., 52, 7680-7688, 2018.

369 Cremer, J. W., Thaler, K. M., Haisch, C., and Signorell, R.: Photoacoustics of single laser-trapped nanodroplets for the direct observation of
370 nanofocusing in aerosol photokinetics, Nature communications, 7, 1-7, 2016.

371 David, G., Parmentier, E. A., Taurino, I., and Signorell, R.: Tracing the composition of single e-cigarette aerosol droplets in situ by laser-
372 trapping and Raman scattering, Scientific reports, 10, 1-8, 2020.

373 Esat, K., David, G., Poulkas, T., Shein, M., and Signorell, R.: Phase transition dynamics of single optically trapped aqueous potassium
374 carbonate particles, Physical Chemistry Chemical Physics, 20, 11598-11607, 2018.

375 Garetz, B. A., Matic, J., and Myerson, A. S.: Polarization switching of crystal structure in the nonphotochemical light-induced nucleation of
376 supersaturated aqueous glycine solutions, Phys. Rev. Lett., 89, 175501, 2002.

377 Garrison, W. M.: Actions of ionizing radiations on nitrogen compounds in aqueous media, Radiation Research Supplement, 4, 158-174,
378 1964.

379 Garrison, W. M.: Radiation-induced reactions of amino acids and peptides, Univ. of California, Berkeley, 1972.

380 George, C., Ammann, M., D'Anna, B., Donaldson, D., and Nizkorodov, S. A.: Heterogeneous photochemistry in the atmosphere, Chem.
381 Rev., 115, 4218-4258, 2015.

382 Girod, M., Moyano, E., Campbell, D. I., and Cooks, R. G.: Accelerated bimolecular reactions in microdroplets studied by desorption
383 electrospray ionization mass spectrometry, Chemical Science, 2, 501-510, 2011.

384 Gong, Z., Pan, Y.-L., Videen, G., and Wang, C.: Optical trapping and manipulation of single particles in air: Principles, technical details,
385 and applications, J. Quant. Spectrosc. Radiat. Transfer, 214, 94-119, 2018.

386 Hall, J. C.: Glycine, Journal of Parenteral and Enteral Nutrition, 22, 393-398, 1998.

387 Homchaudhuri, L. and Swaminathan, R.: Near ultraviolet absorption arising from lysine residues in close proximity: a probe to monitor
388 protein unfolding and aggregation in lysine-rich proteins, Bull. Chem. Soc. Jpn., 77, 765-769, 2004.

389 Jackson, A. A.: The glycine story, Eur J Clin Nutr, 45, 59-65, 1991.

390 Jawor-Baczynska, A., Moore, B. D., Lee, H. S., McCormick, A. V., and Sefcik, J.: Population and size distribution of solute-rich mesospecies
391 within mesostructured aqueous amino acid solutions, Faraday Discuss., 167, 425-440, 2013.

392 Kucinski, T. M., Dawson, J. N., and Freedman, M. A.: Size-Dependent Liquid–Liquid Phase Separation in Atmospherically Relevant
393 Complex Systems, The Journal of Physical Chemistry Letters, 10, 6915-6920, 2019.

394 Lee, J. K., Banerjee, S., Nam, H. G., and Zare, R. N.: Acceleration of reaction in charged microdroplets, Q. Rev. Biophys., 48, 437-444,
395 2015.

396 Lee, J. K., Samanta, D., Nam, H. G., and Zare, R. N.: Micrometer-sized water droplets induce spontaneous reduction, Journal of the American
397 Chemical Society, 141, 10585-10589, 2019.

398 Lundeen, R. A., Janssen, E. M.-L., Chu, C., and McNeill, K.: Environmental photochemistry of amino acids, peptides and proteins, CHIMIA
399 International Journal for Chemistry, 68, 812-817, 2014.

400 Moenig, J., Chapman, R., and Asmus, K. D.: Effect of the protonation state of the amino group on the. cntdot. OH radical induced
401 decarboxylation of amino acids in aqueous solution, The Journal of Physical Chemistry, 89, 3139-3144, 1985.

402 Mopper, K. and Zika, R. G.: Natural photosensitizers in sea water: riboflavin and its breakdown products, in, ACS Publications, 1987.

403 Oraevsky, A. N.: Whispering-gallery waves, Quantum electronics, 32, 377, 2002.

404 Parmentier, E. A., Corral Arroyo, P., Gruseck, R., Ban, L., David, G., and Signorell, R.: Charge Effects on the Photodegradation of Single
405 Optically Trapped Oleic Acid Aerosol Droplets, The Journal of Physical Chemistry A, 126, 4456-4464, 2022.

406 Parmentier, E. A., David, G., Arroyo, P. C., Bibawi, S., Esat, K., and Signorell, R.: Photochemistry of single optically trapped oleic acid
407 droplets, J. Aerosol Sci, 151, 105660, 2021.

408 Pinotsi, D., Buell, A. K., Dobson, C. M., Kaminski Schierle, G. S., and Kaminski, C. F.: A label‐free, quantitative assay of amyloid fibril
409 growth based on intrinsic fluorescence, ChemBioChem, 14, 846-850, 2013.

410 Pöschl, U. and Shiraiwa, M.: Multiphase chemistry at the atmosphere–biosphere interface influencing climate and public health in the
411 anthropocene, Chem. Rev., 115, 4440-4475, 2015.

412 Rapf, R. J. and Vaida, V.: Sunlight as an energetic driver in the synthesis of molecules necessary for life, Physical Chemistry Chemical
413 Physics, 18, 20067-20084, 2016.

414 Reich, O., David, G., Esat, K., and Signorell, R.: Weighing picogram aerosol droplets with an optical balance, Communications Physics, 3,
415 223, 10.1038/s42005-020-00496-x, 2020.

416 Ruiz-Lopez, M. F., Francisco, J. S., Martins-Costa, M. T., and Anglada, J. M.: Molecular reactions at aqueous interfaces, Nature Reviews
417 Chemistry, 4, 459-475, 2020.

418 Shukla, A., Mukherjee, S., Sharma, S., Agrawal, V., Kishan, K. R., and Guptasarma, P.: A novel UV laser-induced visible blue radiation
419 from protein crystals and aggregates: scattering artifacts or fluorescence transitions of peptide electrons delocalized through hydrogen
420 bonding?, Arch. Biochem. Biophys., 428, 144-153, 2004.

421 Sugiyama, T., Yuyama, K.-i., and Masuhara, H.: Laser trapping chemistry: from polymer assembly to amino acid crystallization, Acc. Chem.
422 Res., 45, 1946-1954, 2012.

423 Sun, Z., Zhang, C., Xing, L., Zhou, Q., Dong, W., and Hoffmann, M. R.: UV/nitrilotriacetic acid process as a novel strategy for efficient
424 photoreductive degradation of perfluorooctanesulfonate, Environ. Sci. Technol., 52, 2953-2962, 2018.

425 Swietlicki, E., Hansson, H. C., Hämeri, K., Svenningsson, B., Massling, A., McFiggans, G., McMurry, P. H., Petäjä, T., Tunved, P., Gysel,
426 M., Topping, D., Weingartner, E., Baltensperger, U., Rissler, J., Wiedensohler, A., and Kulmala, M.: Hygroscopic properties of
427 submicrometer atmospheric aerosol particles measured with H-TDMA instruments in various environments—a review, Tellus B: Chemical
428 and Physical Meteorology, 60, 432-469, 10.1111/j.1600-0889.2008.00350.x, 2008.

429 Tang, I. N., Tridico, A. C., and Fung, K. H.: Thermodynamic and optical properties of sea salt aerosols, Journal of Geophysical Research:
430 Atmospheres, 102, 23269-23275, 10.1029/97jd01806, 1997.

431 Terpugov, E. L., Kondratyev, M. S., and Degtyareva, O. V.: Light-induced effects in glycine aqueous solution studied by Fourier transform
432 infrared-emission spectroscopy and ultraviolet-visible spectroscopy, J. Biomol. Struct. Dyn., 39, 108-117, 2021.

433 Tervahattu, H., Tuck, A., and Vaida, V.: Chemistry in prebiotic aerosols: a mechanism for the origin of life, in: Origins, Springer, 153-165,
434 2004.

435 Urquidi, O., Brazard, J., LeMessurier, N., Simine, L., and Adachi, T. B.: In situ optical spectroscopy of crystallization: One crystal nucleation
436 at a time, Proceedings of the National Academy of Sciences, 119, e2122990119, 2022.

437 Walser, M. L., Park, J., Gomez, A. L., Russell, A. R., and Nizkorodov, S. A.: Photochemical aging of secondary organic aerosol particles
438 generated from the oxidation of d-limonene, The Journal of Physical Chemistry A, 111, 1907-1913, 2007.

439 Wang, X., Gemayel, R., Hayeck, N., Perrier, S., Charbonnel, N., Xu, C., Chen, H., Zhu, C., Zhang, L., and Wang, L.: Atmospheric
440 photosensitization: a new pathway for sulfate formation, Environ. Sci. Technol., 54, 3114-3120, 2020.

441 Yuyama, K.-i., Sugiyama, T., and Masuhara, H.: Millimeter-scale dense liquid droplet formation and crystallization in glycine solution
442 induced by photon pressure, The Journal of Physical Chemistry Letters, 1, 1321-1325, 2010.

443 Zaccaro, J., Matic, J., Myerson, A. S., and Garetz, B. A.: Nonphotochemical, laser-induced nucleation of supersaturated aqueous glycine
444 produces unexpected γ-polymorph, Crystal Growth & Design, 1, 5-8, 2001.

445 Zieger, P., Väisänen, O., Corbin, J. C., Partridge, D. G., Bastelberger, S., Mousavi-Fard, M., Rosati, B., Gysel, M., Krieger, U. K., Leck, C.,
446 Nenes, A., Riipinen, I., Virtanen, A., and Salter, M. E.: Revising the hygroscopicity of inorganic sea salt particles, Nature Communications,
447 8, 15883, 10.1038/ncomms15883, 2017.

448 Zimbitas, G., Jawor-Baczynska, A., Vesga, M. J., Javid, N., Moore, B. D., Parkinson, J., and Sefcik, J.: Investigation of molecular and
449 mesoscale clusters in undersaturated glycine aqueous solutions, Colloids Surf. Physicochem. Eng. Aspects, 579, 123633, 2019.

450